

Gravity-driven flows of viscous liquids over two-dimensional topographies

By MICHEL M. J. DECREÉ AND JEAN-CHRISTOPHE BARET

Philips Research Laboratories Eindhoven, 5656 AA Eindhoven, The Netherlands

(Received 22 March 2002 and in revised form 11 December 2002)

Using phase-stepped interferometry, we have measured full two-dimensional maps of the free-surface shape of a thin liquid film of water flowing over an inclined plate with topography. The measurement technique allows us to image automatically the shape of the free surface in a single field of view of about 2.4 by 1.8 mm, with a lateral resolution of 3.1 μm and a height resolution of 0.3 μm . By imaging neighbouring regions and combining them, complete two-dimensional free-surface profiles of gravity-driven liquid films with a thickness ranging between 80 and 120 μm are measured, over step, trench, rectangular and square topographies with depths of 10 and 20 μm , and lateral dimensions of the order of 1 to several mm. The experimental results for both one- and two-dimensional flows are found to be in good agreement with existing models, including a recent two-dimensional Green's function of the linearized problem by Hayes *et al.* This extends the applicability of simple models to cases with a high value of topography steepness and low-viscosity liquids as in our experiments. A corollary of the agreement with the linear two-dimensional model is that our experimental results behave linearly, a convenient property that allows the free-surface response to complex topographies to be worked out from knowledge of the response to an elementary topography like a square.

1. Introduction

The importance of the shape taken by a thin liquid film flowing over a topography has grown with the increasing number of thin film devices that are manufactured. Industries as diverse as microelectronics, displays, optical storage or microfluidic devices all require an understanding of thin liquid film deposition. In most of these products, many layers are successively deposited, photolithographically patterned and developed. As the coating fluid flows, for example by spin, dip or slide coating, its features will be influenced by the previous layer profiles.

Generically, the steady-state problem depicted in figure 1 is to be studied, where a thin film of fluid flows over a topography $T(x, y)$ of typical height T and streamwise length w . The position of the interface with respect to the reference plane $z=0$ is given by $h(x, y)$. The asymptotic film thickness of the film far away from the topography is h_∞ . Gravity is also represented in figure 1, exerting its action at an angle α with the vertical. The extent to which the newly formed film will adopt a profile that conforms to the underlying topography, or on the contrary will planarize, is of prime importance and therefore the problem of thin film flow over a topography has received considerable interest both theoretically and experimentally.

The pioneering theoretical work of Stillwagon, Larson & Taylor (1987) initially studied dried profiles obtained experimentally using a profilometer and was then

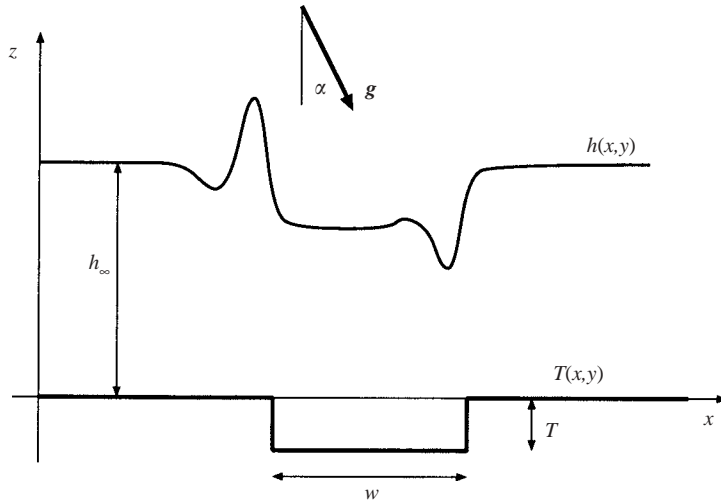


FIGURE 1. Side view of the flow of a thin liquid film of asymptotic thickness h_∞ over a topography $T(x, y)$. The y -axis is oriented perpendicular to the plane of the paper and is therefore not represented. In the case of a one-dimensional problem, each topography step is preceded by a standing capillary wave, and followed by an exponential recovery.

expanded to numerically solve the one-dimensional lubrication equation over shallow trenches in Stillwagon & Larson (1988). They were the first to derive the analytical solution to the one-dimensional lubrication equation for the profile of a film flowing over a step topography (Stillwagon & Larson 1990). They obtained a standing capillary ridge in front of the topography change and a downstream exponential decay. This behaviour is dictated by the interplay of surface tension and body forces, and is characterized by a decay lengthscale hereafter termed the ‘dynamic capillary length’. Later, Roy & Schwartz (1997) extended the one-dimensional lubrication approach of the problem to the case of steep topographies by expressing the problem in a curvilinear coordinate system attached to the substrate (see also Valéry Roy, Roberts & Simpson 2002). Decré, Fernandez-Parent & Lammers (1999) proposed a Green’s function formalism to the problem studied by Stillwagon & Larson (1990), and added a second-order term that causes the capillary ridge to stand more upstream of the topography in the case of deeper topographies. Recently, Kalliadasis, Bielarz & Homsy (2000) reconsidered the problem of topography depths comparable with or larger than the unperturbed film thickness. They solved the corresponding one-dimensional lubrication equation numerically using a dynamical systems approach, showing that deep topographies behave asymmetrically, a step-down causing a comparatively much larger capillary ridge than a step-up. They also showed that gravity could cause the capillary ridge to disappear. Mazouchi & Homsy (2001) completed this work by studying the corresponding Stokes problem, and showed that increasing the importance of viscosity with respect to the surface tension (as expressed by the capillary number Ca , see §3), leads to a widening and flattening of the ridge. Gramlich *et al.* (2002) have also shown that temperature steps superimposed on a one-dimensional topography could, through thermal Marangoni effects, suppress the capillary ridge. The body of literature just discussed provides an extensive, experimentally well-validated analysis of the one-dimensional case. It is a remarkable feature of the lubrication theory as applied to this problem that although its formal

validity is, strictly speaking, limited to the cases of shallow smooth topographies for thin films, or narrow topographies when the film is thicker, it has proven very robust and predictive when compared to experimental results. In a stability analysis of this problem, Kalliadasis & Homsy (2001) have confirmed this behaviour by showing the strong stability of flows over topography with respect to all disturbances (either localized around a topography or disturbances on the film regions away from it, i.e. step changes in flow rate etc.).

The case of two-dimensional topography, has received much less attention so far. Pozrikidis & Thoroddsen (1991) numerically solved the two-dimensional Stokes equation linearized for a small particle topography using boundary integral methods. They obtained results qualitatively identical to the one-dimensional case, with an important capillary ridge standing in front of the obstacle, and two symmetrical, exponentially decaying capillary wakes on the sides. Hayes, O'Brien & Lammers (2000) derived the analytical expression for the Green's function of the linearized two-dimensional lubrication equation over a shallow topography, and obtained free-surface shapes qualitatively comparable to those of Pozrikidis & Thoroddsen (1991). Peurrung & Graves (1991, 1993) studied the decay of the film thickness over a topography in spin coating using an interferometer, and obtained pictures of two-dimensional fringe patterns. They displayed their experimental results next to numerical solutions of the two-dimensional lubrication equation and obtained qualitative agreement. However, Peurrung & Graves (1993) did not extract experimental profiles from their two-dimensional fringe patterns, so no quantitative validation has been available so far.

It is the aim of the present work to provide quantitative full two-dimensional free-surface profiles for the validation of two-dimensional models of thin film flow over a topography. In earlier work, the one-dimensional profiles of thin liquid films flowing over one-dimensional topographies were studied using single-arm interferometry (see Messé & Decré 1997; Lucéa, Decré & Lammers 1999; Decré, Fernandez-Parent & Lammers 1998, 1999). This method relies on measurement of the interference patterns that arise between the wavefront reflected at the surface of the fluid and that reflected at the surface of the substrate. Each dark interference fringe corresponds to destructive interference, and the optical path difference between two neighbouring fringes is then $\Delta s = \lambda / (2n_f \cos \theta_t)$, with λ the wavelength of the analysing beam in air, n_f the refractive index of the fluid, and θ_t the angle of the transmitted light. One therefore obtains information related to the optical path within the fluid film, a quantity proportional to both n_f – the refractive index of the fluid – and h – the local film thickness. A drawback of single-arm interferometry is that it measures the intensity distribution of the wavefront only, i.e. it provides for the position of the interference fringes but not for their phase, as discussed in Hansen (2001). As a consequence, one cannot derive solely from such measurements whether the following fringe corresponds to plus or minus Δs : prior knowledge of the measured profile is needed. The case of a thin liquid film flowing over a one-dimensional topography provides such prior knowledge: first because one-dimensional wavy surfaces cannot contain saddle points, as a surface extremum in a one-dimensional free surface always leads to an inversion of the slope; secondly when studying surfaces on topography, one always knows that the asymptotic levels of the surface up- and downstream of the topography are equal to h_∞ . This knowledge has been used to derive profiles from single-arm intensity interferometry, either manually, Peurrung & Graves (1991) or automatically, Messé & Decré (1997), Decré *et al.* (1999). This technique is however not suited for the analysis of two-dimensional surfaces; in

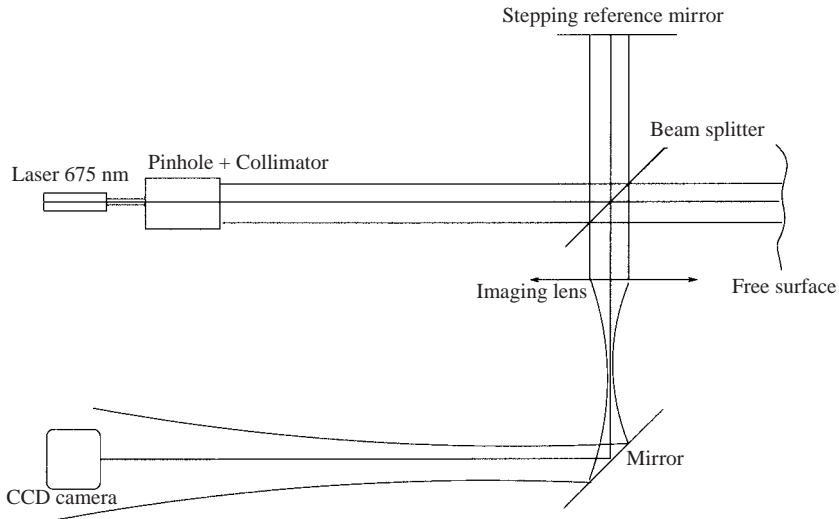


FIGURE 2. Schematic view of interferometric set-up.

general phase indetermination will lead to complex problems around saddle points and in particular the implementation of ‘prior-knowledge’ algorithms into automatic two-dimensional extensions of existing one-dimensional analysis would be restricted to a limited number of cases. This lead us to opt for phase-stepped interferometry, a technique that is routinely used in optical workshops, to determine the phase portrait of optical elements (Gasvik 1996; Malacara, Servin & Malacara 1998), and for which existing software offers automatic computation of the two-dimensional profile.

In the following, we first address the experimental details of phase-stepped interferometry as we applied it to the inclined plate set-up, then we present the results of one-dimensional free-surface profiles before extending to the discussion of two-dimensional profiles. We systematically compare our results to previous theoretical models, and draw a number of conclusions.

2. Experimental

2.1. Optics

Phase-stepped interferometry is used to measure the phase of a wavefront by collecting intensity interferograms for at least three different stepped positions of the reference mirror in a Twyman-Green (or double-arm) interferometer (Gasvik 1996; Malacara *et al.* 1998). The steps must be a fraction of the wavelength of the analysing laser. Here we only sketch the basic principles of the measurement (figure 2). The interested reader is referred to the specialized literature for more details (see references earlier in this paragraph). The time-averaged spatial intensity distribution of an interferogram $I(x, y)$ can be described as a function of the phase of the wavefront $\Phi(x, y)$ using the following equation from Gasvik (1996):

$$I(x, y) = I_0(x, y)[1 + V(x, y) \cos\{\Phi(x, y) - \Phi_r(x, y)\}], \quad (2.1)$$

where $I_0(x, y)$ is the mean intensity, $V(x, y)$ the visibility (representing the local attenuation of the signal), and Φ_r the reference phase determined by the position of the reference mirror. The phase shifted measurements result in a set of intensity maps for different reference phases, the problem being to calculate $\Phi(x, y)$. There are three

unknown quantities in (2.1): $I_0(x, y)$, $V(x, y)$ and $\Phi(x, y)$. In theory, three different measurements of $I(x, y)$ for three known values of Φ_r are sufficient to determine the three unknown quantities, but the calculation is not stable, as is shown in Gasvik (1996). Using four positions z_i of the reference mirror $\Phi_{r,i} = 2\pi z_i/\lambda = 0, \pi/2, \pi, 3\pi/2$ yields a stable scheme and thus the four-step phase $\Phi_4(x, y)$ is given by

$$\Phi_4(x, y) = \arctan\left(\frac{I_2 - I_4}{I_1 - I_3}\right). \quad (2.2)$$

The calculation is performed on each point (x, y) for the complete interferogram. In practice a five-frame algorithm is used, in which a measurement with $\Phi_{r,5} = 2\pi$ is added. The five-step phase $\Phi_5(x, y)$ is now given by

$$\Phi_5(x, y) = \arctan\left(\frac{2(I_2 - I_4)}{I_1 - 2I_3 + I_5}\right). \quad (2.3)$$

The advantage of this five-frame method is that it is immune to second-order nonlinearities of the detector, and phase-shift miscalibration. There is thus a better error compensation. In the following, all measurements were performed using a five-frame scheme.

The details of our set-up are displayed in figure 2. We use a tailored version of a Fisba Optik (St.Gallen, CH) phase-stepped interferometer system, driven with a Philips version of the OMSOft software (Fisba Optik). The beam of our 675 nm diode laser (DLS15, Spindler & Hoyer) is spatially filtered through a 15 μm pinhole, and collimated to a diameter of a few millimetres with an $f = 80$ mm lens. The $f = 400$ mm imaging lens adjusts the magnification $2 < M < 4$ onto the 768×576 pixels monochrome CCD camera (LDH 0703/30, Philips). This magnification is needed in order to resolve the regions of steep profile, where interference fringes have to be resolved with about 20 pixels per fringe. All our lenses have a diameter of 25 mm. Note that we study the shape of the air–water interface of a thin liquid film flowing over a glass plate. Three interfaces generate reflected wavefronts that are the cause of interference: air–water (front), water–glass and glass–air (back). The reference mirror is a 4° glass wedge, serving two goals: first it improves the modulation of the fringes of interest by reducing the impact of the reflections at the water–glass interface; second ghost reflections are removed by the wedged back face. In order to suppress parasitic reflections at the back glass–air interface, an anti-reflection coating tuned at a wavelength of 650 nm has been applied on the glass plate. The reflectivity was lower than 0.2% in a range between 620 and 675 nm, including both HeNe lasers and diode lasers.

It should be noted that the lens numerical aperture puts some limitations on the maximum measurable slope variation of the profile. Any variation in the slope of the measured surface will cause a divergence of the beam. An order of magnitude of the slope of the profile can be estimated in our case by dividing a typical height variation $\delta h \approx 25 \mu\text{m}$ by a typical lateral lengthscale for the capillary waves $L_d \approx 0.8$ mm (L_d will be formally defined in § 3). In our case, when the slope ($O(\delta h/L_d)$) exceeds $25 \mu\text{m}/0.8$ mm, the reflected beam will not be intercepted by the lens and therefore no interference will occur for that region of the profile. Taking as a first-order approximation that the maximum slopes of the profile scales with the topography height T , this puts a limit on the maximum h_∞/T ratio that we can study. We have partly compensated for this problem by adjusting the tilt of the reference mirror, so that topography depths of 20 μm were easily measured. To accommodate deeper

topographies, the numerical aperture of the imaging lens ($NA = D/f = 1/16$ in the present case) should be increased.

Using the five-frame scheme, it takes 0.5 s to register all interferograms, after which the height of the free surface is computed with an accuracy of $0.1\ \mu\text{m}$. The lateral resolution – as determined by the CCD sensor and the magnification – is $3.1\ \mu\text{m}$, safely above the diffraction limit. Since phase-stepped interferometry is an imaging technique, each measurement provides a 768×576 grid with a pitch of $3.1\ \mu\text{m}$. This exceeds our needs, the typical lateral scale of the flow being $L_d \approx 1\ \text{mm}$. We therefore perform a running average on one point out of ten in both x - and y -directions, so that the actual lateral sampling of all profiles displayed hereafter is $31\ \mu\text{m}$. This reduces the size of the data files by a factor 100 without impairing the effective accuracy. It should be noted that for a measurement to succeed, the absolute position of the free surface with respect to the reference mirror must not vary by more than 0.2λ , that is $135\ \text{nm}$, during the whole acquisition of the five interferograms, say 0.5 s. This stringent requirement in terms of flow stability is met using a box to exclude room turbulence, and having the whole set-up installed on a pneumatic anti-vibration system (XL-A, Newport).

Because of the limited field of view of the camera (approx. $2.4 \times 1.8\ \text{mm}$), and the intrinsic large extent of the flow features that follow from the dynamic capillary length $L_d \approx 1\ \text{mm}$, we need to take several pictures by moving the set-up in steps under the interferometer in order to capture the whole profile. The stepping of the set-up is realized with a LabViewTM (National Instruments) program that controls a motorized x-y stage with $2\ \mu\text{m}$ accuracy (Schaad AG, CH). Given that some overlap is needed between neighbouring pictures to support ‘stitching together’, up to 15×15 phase-stepped measurements have to be performed to cover the largest topographies. Such a series can take one hour to acquire, during which the flow conditions have to be kept constant. Small variations in the two-dimensional profile, observed as discontinuities across streamwise stitching bands (see figure 5), can be attributed to small flow rate fluctuations or unsteady variations over the few minutes it takes to scan one band. They are taken account of in our total error budget of $0.3\ \mu\text{m}$.

One significant difference between our previous work on one-dimensional profiles, using single-arm intensity interferograms, is that double-arm phase-stepped interferometry measures the shape of the interface, not the thickness. The overall shape of the underlying substrate will thus also be measured as a slow variation of the interface shape. Since the 1-mm-thick glass plates are clamped upstream, and rest on a steel ball downstream, all at 30° relative to gravity (figure 3), some flexion of the plate can be expected. We have measured this to be satisfactorily approximated with a parabola in the streamwise direction, with a maximum amplitude of $30\ \mu\text{m}$. The residual error after correction is included in the total $0.3\ \mu\text{m}$ already mentioned. The transverse substrate deformation is found to be negligible.

2.2. Inclined plate set-up

We study the flow of a 40-mm-wide demineralized water stream down a $100\ \text{mm} \times 100\ \text{mm} \times 1\ \text{mm}$ glass plate (Dow Corning 7059). The topographies are produced photolithographically by wet-etching the glass and their depths are measured with an optical profilometer (Microfocus, UBM) within $0.1\ \mu\text{m}$. The glass surface is cleaned for 15 min in an ultrasonic bath in demineralized water with 5% vol. Extran soap (Merck) then rinsed successively in demineralized water/ethanol/heptane, as recommended in Pulker (1984). An additional UV-ozone cleaning step of 15 min completes the procedure (PR-100, UVP Inc. USA). The static contact angle of demineralized

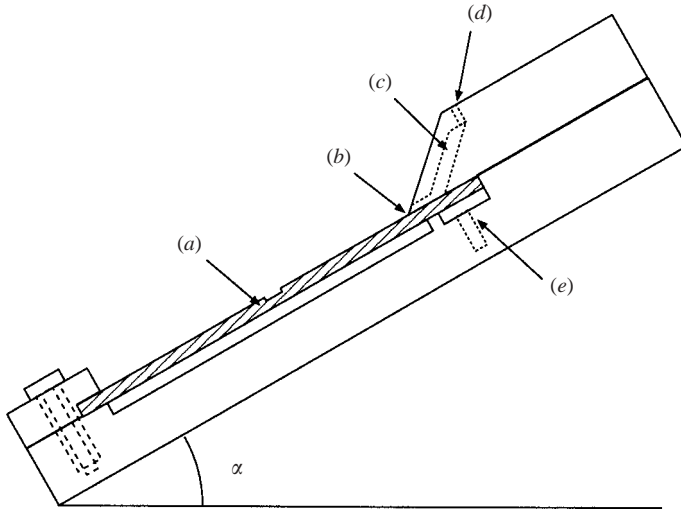


FIGURE 3. Side view of the flow set-up. The entire construction is inclined at an angle α with the horizontal. (a) Glass slide with topography; (b) exit of feeding slit; (c) slit chamber; (d) inlet from reservoir (not displayed); (e) spring-actuated clamping bar (see footnote on p. xxx).

water on such a cleaned glass surface is smaller than 2° (as measured by wedge interferometry, Allain, Ausserré & Rondelez 1985). In order to generate a thin liquid film, we have designed a slit apparatus on an inclined plate (see figure 3). A reservoir feeds the slit chamber by means of a flexible hose. The relative height H of the reservoir with respect to the outlet of the slit determines the pressure head that drives the flow to the underlying plate. A chamber upstream of the slit is purged of all air when starting the flow to obtain stable and reproducible operation. The Poiseuille flow rate through a slit of width b and height d is given by

$$\phi_{slit} = -\frac{1}{12\mu} \frac{dP}{dx} b d^3, \quad (2.4)$$

with μ the dynamic viscosity of the fluid and $dP/dx = -\rho g H/D$ the driving pressure gradient, ρ being the mass density of the fluid, g the acceleration due to gravity and D the streamwise length of the slit. As the fluid has established a steady thin film flow on the inclined plate, the asymptotic film thickness h_∞ is governed by the following lubrication equation for the flow rate:

$$\phi_{plate} = \frac{1}{3\mu} B \rho g \sin \alpha h_\infty^3, \quad (2.5)$$

where B is the actual width of the liquid film on the plate (40 mm) and α is the angle of the plate relative to the horizontal. Considering (2.4) and (2.5), one sees that the asymptotic thickness h_∞ on the plate that is fed through the slit depends on $H^{1/3}$, and is independent of the viscosity of the fluid. In our experiments the height is typically varied between 0.4 m and 1 m. We took care that the height of liquid in the reservoir does not vary more than 2% during an experiment, so that h_∞ is constant within 1%. As we will see later, since the characteristic streamwise scaling length L_d is further proportional to $h_\infty^{1/3}$, our hypothesis of constant operating conditions is valid to better than 0.5%. The slit has $D \times b \times d$ dimensions of 10 mm \times 40 mm \times (25 \pm 1 μ m),

and was cut in an aluminium block. This accuracy allowed us to create a flow with spanwise thickness homogeneity better than 5% †.

Since our interferometric measurements do not provide an absolute value of the position of the interface, we must determine the average flow rate ϕ_{plate} or equivalently the asymptotic thickness h_∞ by other means. We have relied upon both local laser pen profilometry of the free surface (UBM profilometer) and measurements of the liquid height variation in the reservoir to monitor average film height. In a comparison of both techniques, it has been demonstrated (Lucéa *et al.* 1999), that given an accuracy of 0.02 mm in the liquid height H in the reservoir and 0.5 s in time registration, the flow rate was determined within 3%, and provided the width of the film on the plate B was known, the resulting derivation of h_∞ using (2.5) was reliable. Therefore all values of h_∞ reported here have been obtained by measuring the flow rate in the reservoir.

3. Results and discussion

We have studied the flow of water films over a number of topographies – step-up, step-down and trench – across the whole width of the glass plate (one-dimensional) as well as four different rectangular and one square topographies (two-dimensional). The streamwise width of the topographies was $w = 1.2$ mm, with spanwise lengths $L = 1.2, 6, 10, 18$ (two-dimensional) and 100 mm (one-dimensional). The topography depth T was 10 and 20 μm within 0.1 μm . For the demineralized water, we use the following fluid parameters: $\rho = 1000$ kg m $^{-3}$, $\mu = 1$ mPa s and the surface tension $\gamma = 0.070$ N m $^{-1}$. The asymptotic film thickness h_∞ varied between 80 and 120 μm , and the plate was inclined at $\alpha = 30^\circ$ with the horizontal. In the following, we will always discuss dimensionless perturbation profiles $h_1(x, y)/T = (h(x, y) - h_\infty)/T$, to remove the offset caused by the asymptotic thickness h_∞ . The experimental accuracy $\epsilon(h_1/T) = \epsilon(h_1) + \epsilon(T)$ is typically $0.3 \mu\text{m}/20 \mu\text{m} + 0.1 \mu\text{m}/20 \mu\text{m} \approx 2\%$.

As discussed in Kalliadasis *et al.* (2000) and Hayes *et al.* (2000), the dynamic capillary length is the natural in-plane dynamic lengthscale that arises from the lubrication analysis of the problem. The dynamic capillary length L_d can be understood as the film thickness scaled with the capillary number Ca according to $L_d = h_\infty/Ca^{1/3}$, with $Ca = \mu U/\gamma$, U being a characteristic velocity in the film. Following Hayes *et al.* (2000) and Decré *et al.* (1999) our definition of the dynamic capillary length L_d is

$$L_d = \left(\frac{\gamma h_\infty}{3\rho g \sin \alpha} \right)^{1/3}. \quad (3.1)$$

Applying the experimental values mentioned above gives $0.73 \text{ mm} < L_d < 0.83 \text{ mm}$. In the following, all in-plane dimensions will be scaled using L_d , while vertical dimensions will be scaled with T , the topography height. Five dimensional length parameters are present in the problem: film thickness away from the topography, depth, width and length of the topography, and dynamic capillary length. The latter integrates the dynamic quantities as is readily seen from (3.1). Strictly speaking, from these five

† From (2.4) and (2.5), it is seen that $h_\infty \sim d$. The accuracy of the slit height, its reproducibility and its uniformity over the whole width are therefore crucial to the quality of the thin film. We have used a spring-actuated steel bar to uniformly clamp the glass plates with reproducible force against the slit. In practice, the observed flow rates indicate that the actual slit height d is $25 \pm 1 \mu\text{m}$. Any additional fluctuations are due to small particles on the contact surfaces.

dimensional parameters, not more than four dimensionless groups are needed to characterize the problem. A possible set of parameters is the topography width w/L_d , the topography length L/L_d , the dimensionless topography height T/h_∞ and the topography aspect ratio w/T . Taking a closer look at the way Hayes *et al.* (2000) obtained their equation (21), however, shows that this equation apparently contains only two remaining dimensionless parameters: the dimensionless x - and y -extents of the function $T(x, y)$, that correspond to our w/L_d and L/L_d . T/h_∞ is the small parameter of the lubrication problem, and since Hayes *et al.* (2000)'s equation (21) solves for the first-order perturbation of the thickness $h(x, y)$, the small parameter T/h_∞ has been scaled out of the problem (note however that knowledge of T/h_∞ is needed to rebuild the full profile $h(x, y)$ from $h_1(x, y)$ and h_∞). This leaves three independent parameters to be considered, namely w/L_d , L/L_d , and w/T . Since T takes only two values and w a single one (see above), we will not provide w/T hereafter. T/h_∞ , being the 'small parameter', will be given where applicable, for completeness.

We have chosen to work at w/L_d values $O(1)$, to test potential nonlinear effects. Indeed, as discussed by Stillwagon & Larson (1990) and further developed in Kalliadasis *et al.* (2000), when w/L_d is small, the free surface tends to respond to the topography as a localized, singular perturbation, whereas large w/L_d values lead to well-separated non-interacting steps up or down.

3.1. One dimension

Prior to studying two-dimensional features, we reproduced earlier one-dimensional results, putting some emphasis on the case of a trench and a slender rectangle. Figures 4(a) and 4(b) compare the flow over a single step-up and step-down with the linear one-dimensional theory given in Stillwagon & Larson (1990) (equation (12) therein). The film thickness was $h_\infty = 100 \mu\text{m}$ ($T/h_\infty = 0.2$). It can be seen that for the parameter values concerned, the linear one-dimensional theory is excellent, as the r.m.s. difference with the experiments is smaller than the measurement accuracy. Figure 4(c) shows the trench response for $T/h_\infty = 0.19$ ($h_\infty = 105 \mu\text{m}$). Liquid film profiles measured at other film thicknesses of 95 and 113 μm show no quantitative differences. These results confirm, as expected, that such small variations of the thickness – and therefore of the dynamic capillary length – do not influence the response of the flow to the topography. Also here, the linear analytical model shows very good agreement. This confirms our earlier observations from Decré *et al.* (1999) that a weakly nonlinear model is only necessary for T/h_∞ values of the order of 0.5 and larger, and also confirms the more recent analysis by Kalliadasis *et al.* (2000).

3.2. Two dimensions

Figures 5 and 6 present the two-dimensional profiles over topographies with decreasing L/w values of 15, 8.33, 5 and 1 in false colour and perspective, respectively. Classically, Kalliadasis *et al.* (2000) have shown that the response of the free surface for large L/w consists of a ridge upstream of the start of the topography, a fast film height decrease down to a minimum within the trench, and an exponential recovery downstream. The measurements bear great similarity with those of Peurrung & Graves (1991, 1993), bearing in mind that instead of fringe contours, each point in the present work is a measurement. In figure 5, the development of two-dimensional features is clearly seen. For an aspect ratio of 15, the centre of the liquid surface responds as if it were one-dimensional. Some two-dimensional effects have already developed downstream at $L/w = 8.33$, in the form of a curved response in the middle.

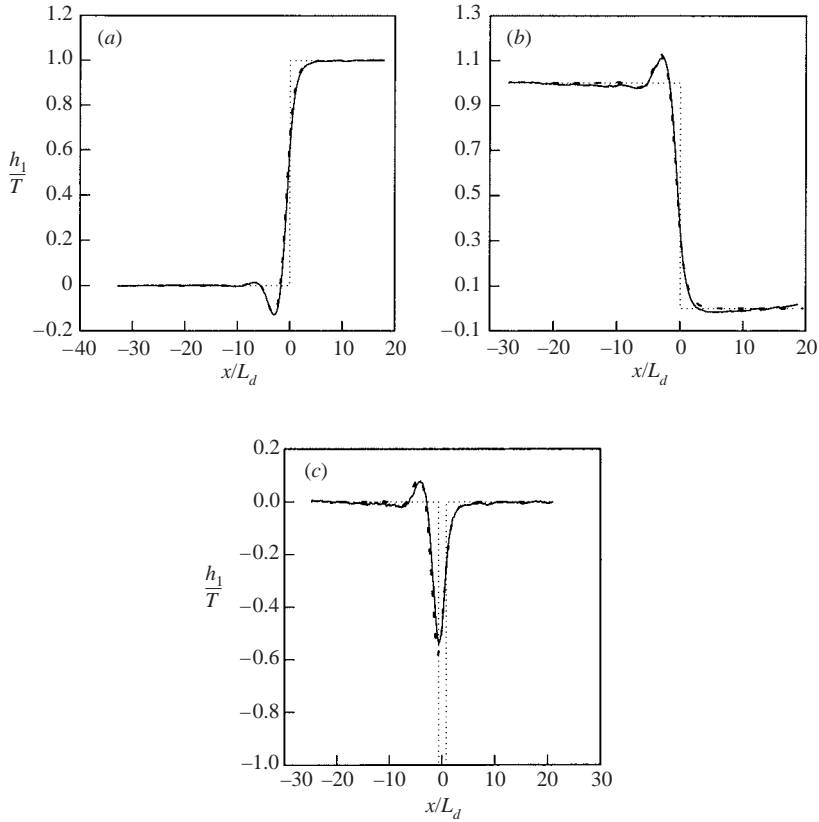


FIGURE 4. Comparison of theoretical (full) and experimental (dashed) liquid film profiles over one-dimensional topography: (a) step-up, $T/h_\infty = 0.22$; (b) step-down, $T/h_\infty = 0.23$; (c) trench, $T/h_\infty = 0.19$, $w/L_d = 1.52$). For reference, the position of the topography is given as a dotted line (refer to figure 1 for relative positions). The r.m.s. difference between experiments and theory is 1.2%.

Over the square, the response is completely two-dimensional and developed. It is only from $L/w \simeq 5$ that the upstream ridge starts to curve.

Figure 6 provides additional qualitative information. The spanwise profile at its deepest point evolves from a more or less flat profile in the centre with edge effects at $L/w = 15$, to a merging of edge effects by $L/w = 8.33$. Narrower topographies cause the deepest profile to narrow even further. Also note the evolution of the streamwise profile on top of the downstream edge of the topography. For $L/w = 15$ it displays three undulations, one in the centre and one on each side, then two undulations on the sides for $L/w = 8.33$, and finally one large central bump for $L/w = 1$.

We now discuss the results on a square in more detail. Figure 7 compares the measured profile h_1 over a square ($w/L_d = 1.54$ and $T/h_\infty = 0.25$) and the theoretical response to a Dirac topography, $h_{1,\delta}$ following Hayes *et al.* (2000). The theoretical profile has been scaled with the volume of the topography $w^2 \times T$, equivalent to assuming that the topography can be expressed as $T(x, y) = w^2 T \delta(x, y)$, with $\delta(x, y)$ the two-dimensional Dirac function. Both pictures are displayed at the same scale. The theoretical profile has been obtained by numerical integration of equation (86) in Hayes *et al.* (2000), using the computer algebra software Mathematica (Wolfram

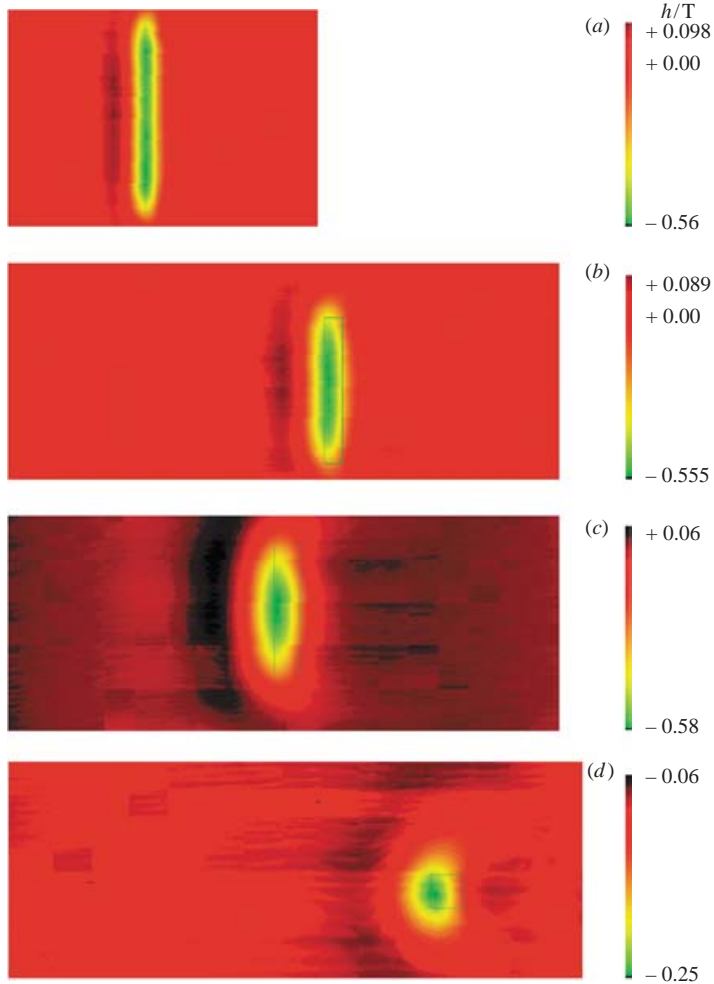


FIGURE 5.

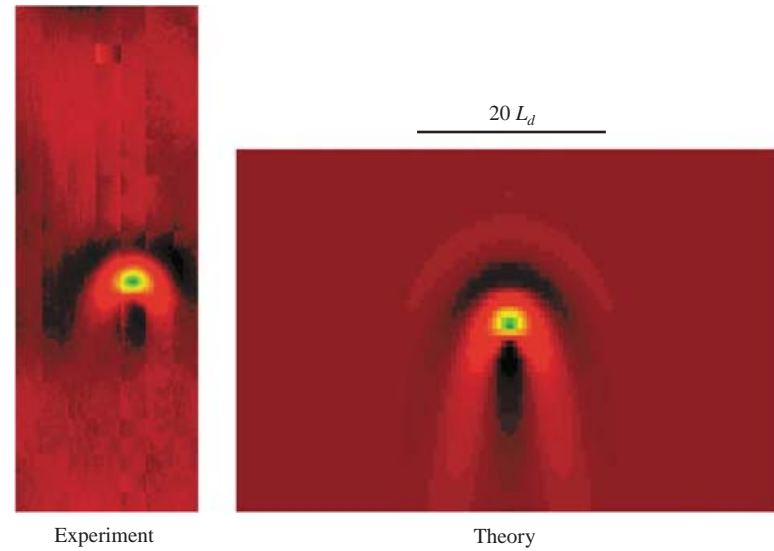


FIGURE 7. False colour representation of the free surface over a square. Comparison between theory and experiment. All scales, lateral and vertical, are the same. Background red: $h_1/T \approx 0$; dark red: $h_1/T > 0$; dark green: $h_1/T < 0$. $w/L_d = 1.54$, $T/h_\infty = 0.25$. Flow is from top to bottom.

FIGURE 5. False colour mapping of the free surface for decreasing aspect ratios L/w of the feature. T/h_∞ : (a–c) 0.15, (d) 0.25; L/w : (a) 15; (b) 8.33; (c) 5; (d) 1. The topography is delineated on scale as a green line. $w/L_d \approx 1.52$. Flow is from left to right.

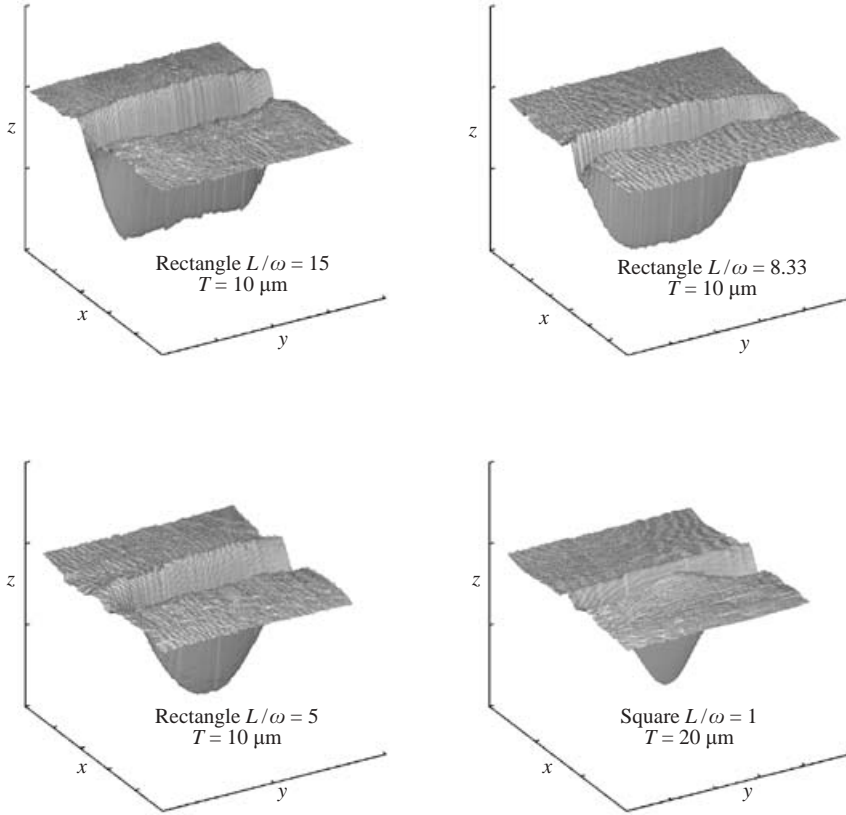


FIGURE 6. Shape of the free surface for decreasing aspect ratios L/w . x is streamwise direction and y spanwise direction. For dimensionless parameters see figure 5.

Inc.). The value of $h_{1,\delta}$ was calculated over the (x, y) domain $[(-50, 50), (0, 50)]$, using the (x, z) -plane symmetry, and care has been taken to verify that the integral of $h_{1,\delta}$ was equal to 1, to avoid errors in scaling. We have checked that the one-dimensional profiles computed over a one-dimensional topography using the two-dimensional $h_{1,\delta}$ are in agreement with the standard, analytical one-dimensional linear theory.

The qualitative agreement in figure 7 is striking, as it is also with figures 3 and 9 from Pozrikidis & Thoroddsen (1991). Note that the experimental profile is more spread out than the theoretical Dirac response, which can be attributed to the finite dimensions of the actual topography.

Figures 8 and 9 show respectively streamwise and spanwise experimental profiles taken from figure 7, at intervals of half a topography width $w/(2L_d)$.

The theoretical profiles in figures 8 and 9 are computed numerically using convolution on $h_{1,\delta}$, according to Hayes *et al.* (2000):

$$\left. \begin{aligned}
 h_1(x, y) &= \int_{-\infty}^{\infty} \int_{-\infty}^{\infty} T(x_0, y_0) h_{1,\delta}(x - x_0, y - y_0) dx_0 dy_0, \\
 T(x, y) &= -1 \quad \text{for } -w/(2L_d) \leq x \leq w/(2L_d), \quad -w/(2L_d) \leq y \leq w/(2L_d), \\
 T(x, y) &= 0 \quad \text{for } x, y < -w/(2L_d), \quad x, y > w/(2L_d).
 \end{aligned} \right\} \tag{3.2}$$

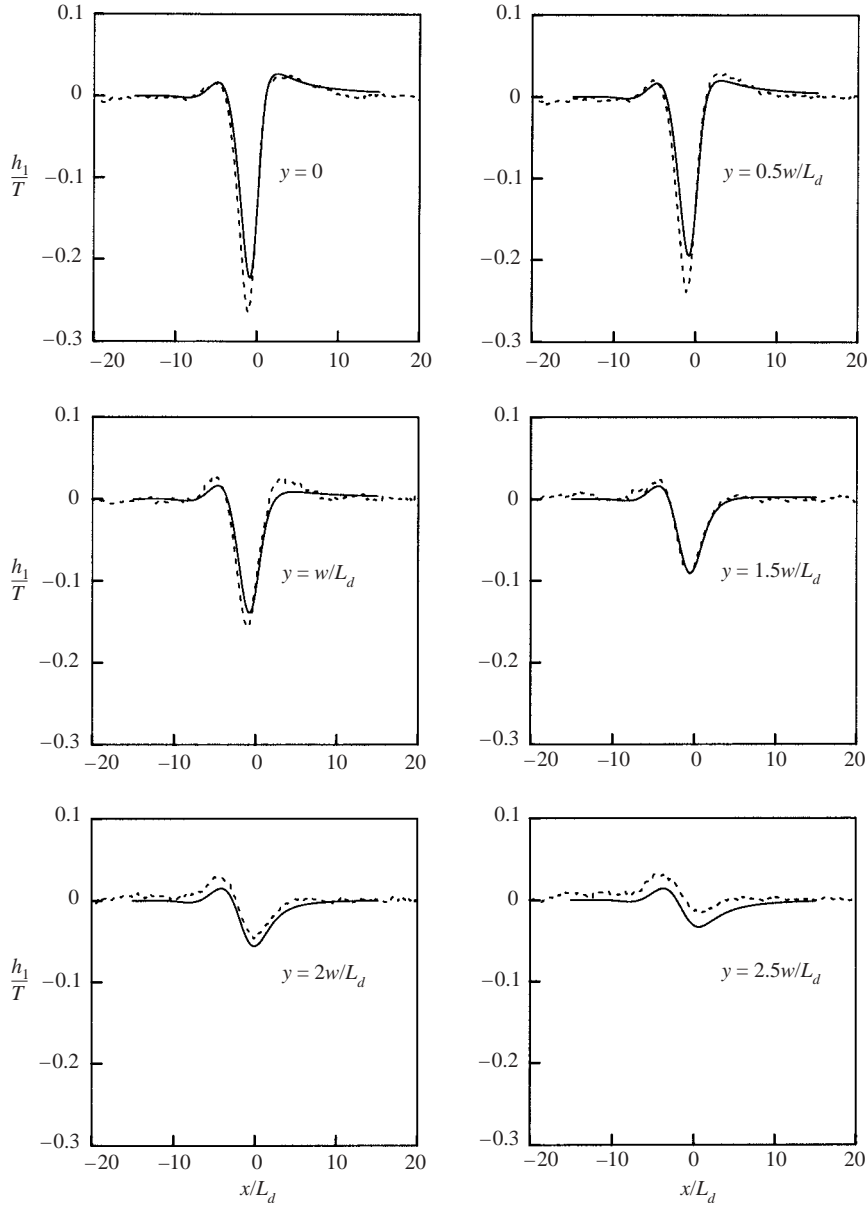


FIGURE 8. Comparison of experimental (dashed) streamwise (x) free-surface profiles with theory (full), for several y positions in the case of a square topography, $w/L_d = 1.54$, $T/h_{\infty} = 0.25$.

Both the positions of the extrema and their amplitudes are in very good agreement. Note that the noise observed, particularly in figure 9, though significant, represents less than $0.01T$ (that is $0.2 \mu\text{m}$).

Linearity is a very useful property that allows profiles of complex topographies to be built from the linear addition of the response to a single building block. It is thus interesting to verify to what extent our experimental results indeed behave linearly, beyond their comparison with the linear theory. The response on a rectangular topography for $L = 5w$ can be obtained by the linear summation of the response on

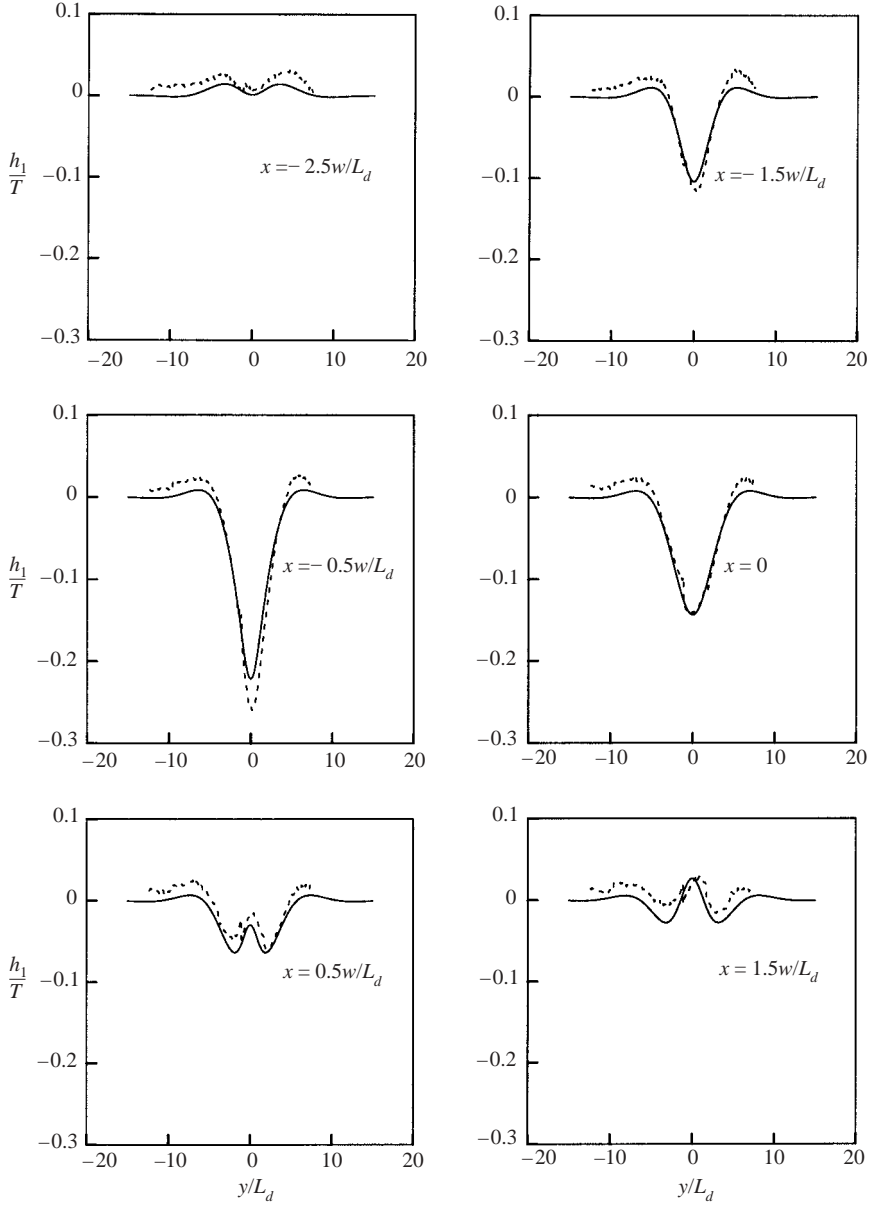


FIGURE 9. Comparison of experimental (dashed) spanwise (y) free-surface profiles with theory (full), for several x positions in the case of a square topography, $w/L_d = 1.54$, $T/h_\infty = 0.25$.

a square topography (figure 10):

$$h_1^{L=5w} = \sum_{i=-2}^2 h_1^{sq}(x, y + i \times w/L_d), \quad (3.3)$$

where i corresponds to the numerals in figure 10. Note that (3.3) is easily generalized to any arbitrary combination of squares. As a consequence, from measurements of the profiles $h_1^{sq}(x, y)$ on a single square as discussed previously, one can calculate the

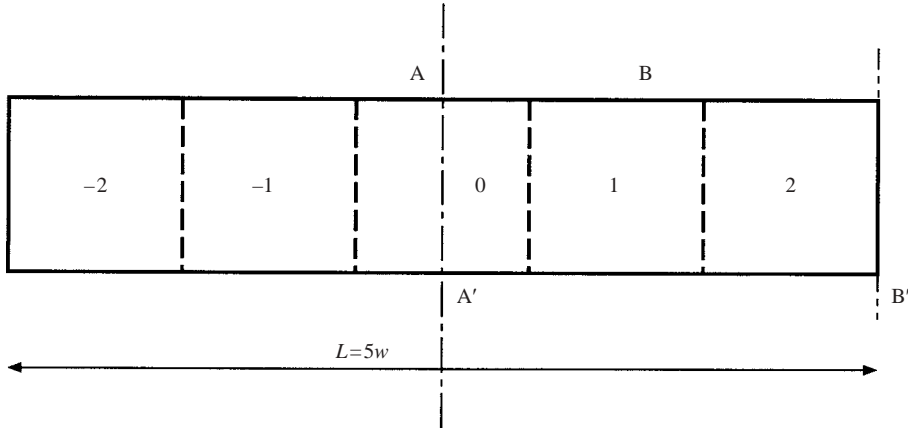


FIGURE 10. Concept of the linearity test. Five squares of size w identified by roman numerals make up a rectangle of width $L = 5w$. Centre cross-section AA' and side cross-section BB' (see text for explanation).

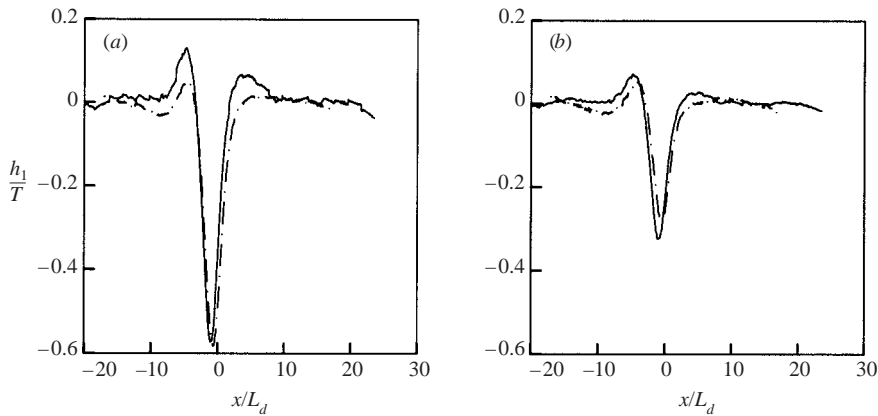


FIGURE 11. Experimental test of the linearity: comparison of the linear summation of experimental square profiles (full) with the equivalent $L = 5w$ rectangle (dot-dashed) streamwise profiles. (a) $y = 0$, (b) $y = 2.5w/2L_d$.

sum in (3.3) and compare it with the experimental results for a rectangle $L = 5w$. We have done this for the centre-profile $h_1^{L=5w}(x, 0)$ (cross-section AA' , figure 10), and for the side-profile $h_1^{L=5w}(x, 2.5w/L_d)$ (cross-section BB' , figure 10) with very good agreement as shown in figure 11.

It follows from the preceding results that the experimental system behaves linearly for the range of parameters discussed here, and that linear superposition of profiles obtained from elementary topographies can be used to construct more complex structures.

In the light of this, the actual experimental conditions can be compared with the validity limits of the linearized lubrication approximation used in Hayes *et al.* (2000). Let us first introduce some dimensionless groups: the modified Reynolds number $Re T/\delta$, with $Re = \rho U h_\infty/\mu$, δ being a typical distance that characterizes the steepness of the topography (see e.g. δ^* in Kalliadasis *et al.* 2000); the gravity parameter

h_∞ [μm]	80	120
U [m s^{-1}]	0.03	0.07
Ca	0.4×10^{-3}	1.1×10^{-3}
Bo	0.8×10^{-3}	1.7×10^{-3}
G	0.15	0.17
T [μm]	10 20	10 20
ReT/δ	12 24	18 36
$Ca^{2/3}h_\infty T/\delta^2$	1.16 2.31	3.2 6.4

TABLE 1. Relevant dimensionless numbers for the present experiments

$G = Bo Ca^{-2/3} \approx 1$, with the Bond number $Bo = \rho g h_\infty^2 / \sigma$. A number of conditions can be found in the literature for the validity of the lubrication equation in our case:

- (a) when $Ca \approx 1$, Stokes' equation should be used (see Mazouchi & Homsy 2001);
- (b) inertia terms are needed when $Re T/\delta \approx 1$;
- (c) when $G = Bo Ca^{-2/3} \approx 1$ the gravitation component normal to the substrate should be included (see Kalliadasis *et al.* 2000);
- (d) when $Ca^{2/3}h_\infty T/\delta^2 \approx 1$ Roy & Schwartz (1997) describe the flow in a curvilinear system attached to the substrate.

Table 1 displays the values of the various cited dimensionless groups for our experimental conditions. It appears that while Ca and G are small enough not to require Stokes' equation or normal gravitation corrections, both the corrected Reynolds number and the topography slopes are significantly high. These conditions apply to with the low viscosity liquid we study†. Strictly speaking, one should consequently use both an orthogonal curvilinear coordinate system and inertia terms to describe the experimental results observed here. In particular, the topography and its first three derivatives should all vary over lengthscales that are long compared to the local film thickness, which is in contradiction with our very steep topographies, $\delta/T \approx 1/5$. However, the very good agreement of experiments with the two-dimensional linear lubrication model by Hayes *et al.* (2000) that we present here provides a strong indication that if topography slope and inertia have an effect, it will be small.

To conclude, we shall discuss some specific features observed here in the case of a two-dimensional topography. A striking difference between one-dimensional and two-dimensional topographies is that the former have a limited effect downstream of the last step feature, while the latter display long perturbations in the wake of the topography.

When dealing with coating liquids that contain a solute, minute thickness variations can trigger concentration gradients during the final coating formation, e.g. because of solutal Marangoni flows, as discussed in Eres, Weidner & Schwartz (1999). One can therefore expect the wake of a localized perturbation in a thin film flow to develop long perturbed tails on both sides. Such a feature is commonly known in coating technology practice as a comet-tail (see e.g. figure 4 in Hayes *et al.* 2000). Obtaining a quantitative model for the description of such comet-tails may be achieved in the

† Note that since the mean flow velocity U is inversely proportional to the viscosity μ , the capillary number $Ca = \mu U / \sigma$ is independent of the viscosity. Therefore, one could study higher viscosity liquids without increasing Ca , while reaching conditions closer to ideal lubrication. As we have noted in the introduction however, practical considerations lead to our interest in systems with lower viscosities.

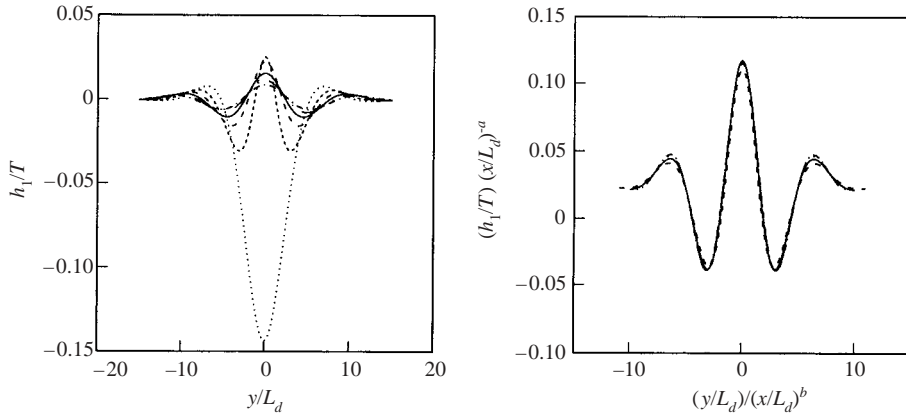


FIGURE 12. (a) Evolution of the spanwise (y) theoretical profile in the wake of a square of width $w = 1.5L_d$. (b) Re-scaled spanwise profiles for $x > 2L_d$: the collapse on a single curve shows that the profiles are self-similar. \dots , $x = 0$; $---$, $x = 2L_d$; $---$, $x = 4L_d$; $-$, $x = 6L_d$; $-\cdot-$, $x = 8L_d$; $-\cdot-\cdot-$, $x = 10L_d$.

future by extending the two-dimensional Green's function model with evaporation terms or resorting to numerical analysis as in Eres *et al.* (1999).

In the case of one-dimensional topographies, the local curvature of the substrate causes a standing capillary ridge upstream of the step-down topography (see e.g. discussion in Kalliadasis *et al.* 2000), followed by an exponential relaxation downstream of the topography, with L_d as the characteristic lengthscale: after a distance of $3L_d$ the perturbation has decayed to less than 5% of its maximum (figure 4). The situation is different in the two-dimensional case: here also, a capillary ridge arises upstream of the step-down topography, see the bow-shaped dark region in figure 7. However this time, the localized pressure peak leads to a negative pressure gradient outwards in all directions, instead of along the x -axis only. Along the streamwise direction, the behaviour remains very much like that of a one-dimensional topography, with the notable exception of a second capillary surge downstream of the step-up topography (see figure 8, $y = 0w/L_d$: this downstream capillary surge is higher and decays more slowly than the upstream ridge). On the sides of the topography, a spanwise perturbation is created that relaxes very slowly in the wake of the localized topography, as illustrated in figure 12 (left). We believe that this 'horseshoe'-shaped bow-ridge comes from two combined effects: first the localized pressure gradient in the upstream ridge drives liquid sideways, away from the adverse pressure gradient; and secondly, the advective terms bend the liquid downstream, leading to the horseshoe shape. The cause of the downstream surge is not very clear to us, although we conjecture that the introduction of the coupled x - and y -derivative terms due to surface tension in the governing equation, dictates oscillatory modes along y , so that the two sidearms of the bow-ridge have to be smoothly connected and form a decaying spanwise wave as seen in figure 12(a). The evolution of the spanwise profiles downstream of a square shows that lateral thickness variations of a few percent are still present at a distance of ten times the dynamic capillary length L_d , much slower than in the one-dimensional case. This behaviour was present in Hayes' Green's function and can be quantitatively described. According to Hayes *et al.* (2000), the Green's function $G(x, y)$ is solution of the equation

$$\partial_x G + \partial_{xxx} G + 2\partial_{xyy} G + \partial_{yyy} G = \delta(x)\delta(y). \quad (3.4)$$

Far away from the δ -topography, $\partial_{xxyy}G$ and $\partial_{xxxx}G$ are negligible compared to $\partial_{yyyy}G$. The behaviour of the film is then given by the balance of the two terms: $\partial_x G = -\partial_{yyyy}G$. To solve this equation, a Fourier transformation can be performed on the y variable. After integration on the x variable and inverse Fourier transformation, it is found that $G(x, y)$ will have a self-similar behaviour according to $G(x, y) \propto x^{-a} f(y/x^b)$, with $b = 1/4$ and $a = b + 1 = 5/4$; f is a function depending only on the parameter y/x^b . One can expect this power-law behaviour for the thickness of the film far downstream of a topography. In figure 12(b) we have applied the scaling $y' = y/x^b, h' = x^a h$ in order to collapse all the experimental curves onto a single master-curve. The optimal scaling exponents for these curves were found to be $a = 1.1$ and $b = 0.23$ which is of the expected order of magnitude for these exponents. The difference with the Green's function scaling exponents is due to the spatial extent of the topography that induces higher-order terms which interfere in the scaling. This analysis shows that the perturbations observed after a two-dimensional localized topography are decreasing following a power-law scaling. The small value of the exponent a explains why the perturbation remains in the flow over long distances. Exponent b represents the divergence of the two arms of the tail. Once again the small value of this exponent shows that the tail will spread slowly in the y -direction.

Due to its ease of use by convolution with elementary topographies and its linearity, the experimentally validated analytical two-dimensional Green's function obtained by Hayes *et al.* (2000) should contribute to a better insight into numerous practical coating problems. Also, we believe that the 'inverse problem', where the topography providing a desired film thickness profile is obtained, would be an interesting problem in the future, as it would provide the coating engineer with topography solutions and further insight into which topographies minimize problems like the capillary ridge in one dimension or the horseshoe bow and downstream surge in two dimensions.

4. Conclusions

In the present work, phase-stepped interferometry has been applied for the first time to the measurement of complete two-dimensional maps of the free-surface shape of thin liquid films flowing over a topography. The measurement technique allows us to attain unprecedented height accuracy and lateral resolution for steady-state film flows. We have applied this technique successfully to the experimental analysis of the quantitative changes in the film height as the underlying topography goes from one- to two-dimensional. The results show that two-dimensional effects are essentially localized at the edges of the topography when its aspect ratio L/w is above 5. In this case, the shape of the interface in the centre part of the topography is described well using existing one-dimensional lubrication theory. The case of a square topography has successfully been compared with a recently published linear two-dimensional lubrication model. We use square profiles to demonstrate that the system still behaves linearly in our parameter range. Although dimensionless groups indicate that the lubrication approximation is not exactly appropriate in our case, and one should incorporate a curvilinear coordinate system and inertia terms, the very good agreement obtained with the two-dimensional lubrication model shows that such effects should be weak. We also show that in contrast with the one-dimensional case, the effects of a two-dimensional topography will be felt far downstream of the topography, according to a power-law relaxation.

Future experiments using higher-viscosity liquids could provide a broader validation of the two-dimensional lubrication theory.

Finally, we suggest an experimental technique to measure both the thickness distribution of the film and the solute concentration in evaporating films. By combining the present phase-stepped interferometry with single-arm interferometry as used earlier by Peurrung & Graves (1991) and Decré *et al.* (1999), it should be possible to obtain both the thickness distribution of the film and its local index of refraction. Since the latter is related to the solute concentration, such combined measurements should provide two-dimensional measurements of both the thickness and the concentration, allowing the detailed study of evaporating flows over topography.

We would like to thank our colleagues J. H. Lammers for stimulating discussions, F. Zijp for invaluable help in developing the phase-stepped interferometer, as well as P. C. Duineveld and H. van Tongeren for their careful review of the manuscript.

REFERENCES

- ALLAIN, C., AUSSERRÉ, D. & RONDELEZ, F. 1985 A new method for contact-angle measurements of sessile drops. *J. Colloid Interface Sci.* **107**, 5–13.
- DECRÉ, M. M. J., FERNANDEZ-PARENT, C. & LAMMERS, J. H. 1998 Flow of a gravity driven thin liquid film over one-dimensional topographies. *Philips Research Unclassified Rep.* NL-UR 823/98.
- DECRÉ, M. M. J., FERNANDEZ-PARENT, C. & LAMMERS, J. H. 1999 Flow of a gravity driven thin liquid film over one-dimensional topographies: a tripartite approach. In *Proc. 3rd European Coating Symposium* (ed. F. Durst & H. Raszillier), pp. 151–156. Shaker.
- ERES, M. H., WEIDNER, D. E. & SCHWARTZ, L. W. 1999 Three-dimensional direct numerical simulation of surface-tension-gradient effects on the leveling of an evaporating multi-component fluid. *Langmuir* **15**, 1859–1871.
- GASVIK, K. J. 1996 *Optical Metrology*, 2nd edn. Wiley & Sons.
- GRAMLICH, C. M., KALLIADASIS, S., HOMSY, G. M. & MESSER, C. 2002 Optimal leveling of flow over one-dimensional topography by Marangoni stresses. *Phys. Fluids* **14**, 1841–1850.
- HANSEN, R. F. 2001 Radar interferometry, Data interpretation and error analysis. PhD Thesis, Technische Universiteit Delft.
- HAYES, M., O'BRIEN, S. B. G. & LAMMERS, J. H. 2000 Green's function of steady flow over a two-dimensional topography. *Phys. Fluids* **12**, 2845–2858.
- KALLIADASIS, S., BIELARZ, C. & HOMSY, G. M. 2000 Steady free-surface thin film flows over topography. *Phys. Fluids* **12**, 1889–1898.
- KALLIADASIS, S. & HOMSY, G. M. 2001 Stability of free-surface thin-film flows over topography. *J. Fluid Mech.* **448**, 387–410.
- LUCÉA, M., DECRÉ, M. M. J. & LAMMERS, J. H. 1999 Flow of a gravity driven thin liquid film over topographies. *Philips Research Unclassified Rep.* NL-UR 833/99.
- MALACARA, D., SERVIN, M. & MALACARA, Z. 1998 *Interferogram Analysis for Optical Testing*. Marcel Dekker.
- MAZOUCHI, A. & HOMSY, G. M. 2001 Free surface Stokes flow over topography. *Phys. Fluids* **13**, 2751–2761.
- MESSÉ, S. & DECRÉ, M. M. J. 1997 Experimental study of a gravity driven water film flowing down inclined plates with different patterns. *Philips Research Unclassified Rep.* NL-UR 030/97.
- PEURRUNG, L. M. & GRAVES, D. B. 1991 Film thickness profiles topography in spin coating. *J. Electrochem. Soc.* **138**, 2115–2124.
- PEURRUNG, L. M. & GRAVES, D. B. 1993 Spin coating over topography. *IEEE Trans. Semi. Man.* **6**, 72–76.
- POZRIKIDIS, C. & THORODDSSEN, S. T. 1991 The deformation of a liquid film flowing down an inclined plane wall over a small particle arrested on the wall. *Phys. Fluids A* **3**, 2546–2558.
- PULKER, H. K. 1984 *Coatings on Glass*. Elsevier.
- ROY, R. V., & SCHWARTZ, L. W. 1997 Coating flow over a curved substrate. In *Proc. 2nd European Coating Symposium* (ed. P. G. Bourgin), pp. 18–27. Université Louis Pasteur, Strasbourg.
- STILLWAGON, L. E. & LARSON, R. G. 1988 Fundamentals of topographic substrate levelling. *J. Appl. Phys.* **63**, 5251–5228.

- STILLWAGON, L. E. & LARSON, R. G. 1990 Leveling of thin films over uneven substrates during spin coating. *Phys. Fluids A* **2**, 1937–1944.
- STILLWAGON, L. E., LARSON, R. G. & TAYLOR, G. N. 1987 Planarization of substrate topography by spin coating. *J. Electrochem. Soc.* **134**, 2030–2037.
- VALÉRY ROY, R., ROBERTS, A. J. & SIMPSON, M. E. 2002 A lubrication model of coating flows over a curved substrate in space. *J Fluid Mech.* **454**, 235–261.